J. Wind Eng. Ind. Aerodyn. 135 (2014) 76–89

Contents lists available at ScienceDirect

Journal of Wind Engineering and Industrial Aerodynamics

journal homepage: www.elsevier.com/locate/jweia

Influence of operating conditions on unsteady wind performance of vertical axis wind turbines operating within a fluctuating free-stream: A numerical study

David Wafula Wekesa [a,b,*], Cong Wang [a], Yingjie Wei [a], Louis Angelo M. Danao [c]

[a] Institute of Dynamics and Control of Spacecrafts, School of Astronautics, Harbin Institute of Technology, Harbin City, PR China
[b] Department of Physics, Jomo Kenyatta University of Agriculture & Technology, Nairobi City, Kenya
[c] Department of Mechanical Engineering, University of the Philippines, Diliman, Quenzon City, Philippines

ARTICLE INFO

Article history:
Received 25 June 2014
Received in revised form
24 September 2014
Accepted 17 October 2014
Available online 5 November 2014

Keywords:
Unsteady wind
VAWT
CFD
Power coefficient
NACA00XX

ABSTRACT

A fluctuating free-stream in unsteady wind environment presents a more significant challenge in wind turbine performance. In this paper, a numerical method is presented to investigate the influence of operating conditions on Vertical Axis Wind Turbine (VAWT) of NACA00XX symmetric airfoils with 12% and 22% thickness in unsteady wind condition. The Computational Fluid Dynamics (CFD) numerical method was used to analyze the aerodynamic performance and physics of flow of the VAWT. The VAWT dynamic motion of blades was introduced by sinusoidally oscillating both VAWT blades. Using a validated CFD model, steady wind simulations at $U_{mean}=7.00$ m/s and 11.00 m/s were conducted and the results predicted the Power Coefficient (CP) performance for the VAWT scale. The results derived in the numerical analysis show that, within fluctuating free-stream wind conditions, thicker airfoils are desirable. Overall maximum unsteady CP of VAWT with thicker blades reveals positive deviations if the tip speed ratio λ is slightly higher than λ of the steady maximum CP, while thinner blades maximum CP marginally drops from the steady maximum CP for the same λ range. Higher frequencies of fluctuation marginally improve the unsteady wind performance of both VAWT blade profiles. High fluctuation amplitudes reveal overall performance degradation on both VAWT blade profiles more than small fluctuation amplitudes. The findings lend substantially to our understanding of both the kinematic and aerodynamic behavior on VAWT scale blades operating in unsteady wind condition, and the flow physics that causes the behavior.

1. Introduction

There is a high demand for sustainable methods of electric power production. This is attributable to finite supply and environmental impacts of fossil fuel (Aslam Bhutta et al., 2012; Wakui and Yokoyama, 2013). The wind energy has been one of the veritable alternative resources for power production over the last decade because wind turbines offer the potential for carbon free power generation (Mullen and Hoagg, 2013; Danao et al., 2013).

The application of small wind turbines for decentralized electricity generation within cities has been on increase contributing to the energy needs of both isolated and grid connected consumers (Monteiro et al., 2013). Compared to the horizontal axis wind turbines, the Vertical Axis Wind Turbines (VAWTs) can be effectively used in urban areas where wind has characteristics of unsteadiness with turbulence (Scheurich and Brown, 2013; Scheurich, 2011; Edwards et al., 2012). The VAWT can be broadly divided into three basic types, namely: Savonius type, Darrieus type, and Giromill type. In the small-scale wind turbine market, the simple straight-bladed Darrieus VAWT is preferred due to its simple blade design (Islam et al., 2008).

Theoretical researches on wind engineering can be categorized into analytical and numerical calculations (Qunfeng et al., 2011). But it is still very difficult to fully solve a flow problem by analytical calculation method. Numerical methods can be classified into two types, namely: The Computational Fluid Dynamics (CFD) methods that analyze directly the flow around the blade of a wind turbine; and the Blade Element Momentum (BEM) method that uses the lift and drag coefficients of each airfoil element with the local geometry and design flow conditions to predict aerodynamic performance (Roh and Kang, 2013; Bedon et al., 2013;

* Corresponding author at: Institute of Dynamics and Control of Spacecrafts, School of Astronautics, Harbin Institute of Technology, Harbin City, PR China. Tel.: +86 15734612395/+254 725037264.
E-mail addresses: dwekesahit@gmail.com, david_@hit.edu.cn (D.W. Wekesa).

http://dx.doi.org/10.1016/j.jweia.2014.10.016
0167-6105/

Song and Lubitz, 2014; Refan and Hangan, 2012). The CFD methods have the ability to model fluid flow in complex geometries, and solve the governing fluid flow equations at thousands of positions on and around the blade in an iterative process (Burton et al., 2011).

Consul et al. (2009), investigated solidity by use of a 2D CFD method to model a two-bladed and four-bladed VAWTs using National Advisory Committee for Aeronautics (NACA) 4-digit (00XX) series symmetric airfoil of NACA0015 profile with corresponding solidities $\sigma=0.019$ and $\sigma=0.038$. The solidity σ, can be expressed conventionally as [see Edwards et al. (2012), Consul et al. (2009), Goude and Ågren (2014)]

$$\sigma = \frac{Nc}{R_{rotor}} \tag{1}$$

where N is the number of rotor blades, c is the blade chord, and R_{rotor} is the rotor radius of the VAWT. Various tip speed ratios from $\lambda=3$ to $\lambda=8$ were analyzed to determine the effects of varying solidity on VAWT aerodynamic performance at steady inflow, where λ is the tip speed ratio expressed as [see Hameed and Afaq (2013), McTavish et al. (2013a)]

$$\lambda = \frac{\omega R_{rotor}}{U_\infty} \tag{2}$$

where ω is rotational velocity of VAWT in a flow of free stream wind speed U_∞. From the study, entire performance curve of the higher solidity VAWT was shifted to the left attributable to the decrease in streamwise velocity presented with lower angles of attack. Their results were similar to investigations in Eboibi et al. (2013), Sheldahl and Klimas (1981), Danao et al. (2012).

Healy (1978) developed a multiple stream tube model for the VAWT, and conducted an analysis of the effects of thickness and camber on VAWT performance. It was concluded that thicker airfoils performed better, especially at a lower Reynolds number, due to their resistance to stall. The work contradicted studies performed in Consul et al. (2009), Hameed and Afaq (2013), Eboibi et al. (2013), Danao et al. (2012), where thinner airfoils, through stronger pressure gradients, produced higher values of lift.

However, for all works in Hameed and Afaq (2013), Eboibi et al. (2013), Danao et al. (2012), Healy (1978), Mcintosh (2009), the CP-λ performance simulations were conducted using a steady inflow, hence the VAWTs unsteady aerodynamic loading induced by the unsteady wind inflow was isolated. This was attributed to lack of substantive work regarding VAWT performance in unsteady wind inflow (Danao et al., 2013, 2014).

The complexity of the airflow around vertical blades as well as the resulting dynamic effects on the rotor have motivated researchers to develop several approaches with the aim of estimating the behavior and the performance of this particular turbine (Danao et al., 2014; Bedon et al., 2014). The recent substantive study carried out by Danao et al. (2014) is a big break through in the H-rotor type VAWTs under fluctuating conditions. The aerodynamic performance and the flow physics surrounding VAWT blades in unsteady winds were investigated. However, the influence of operating conditions on VAWTs with different blade profiles, operated in unsteady winds, was not considered.

Therefore, in this study, a CFD numerical method was used to examine unsteady wind performance on VAWT operating in unsteady wind condition of NACA00XX symmetric airfoils with 12% and 22% thickness. The influence of operating conditions on unsteady wind performance of VAWT blade profiles, which dictates the point and time of stall on a blade, has been analyzed. In addition, the study provides detailed understanding of both the kinematic and aerodynamic behavior on a VAWT blade, and the flow physics that causes the behavior.

2. Blade kinematics and aerodynamics

Straight-bladed darrieus type VAWT is known for its effectiveness in urban areas where wind has characteristics of unsteadiness with turbulence (Tai et al., 2013). However, both the kinematics and aerodynamics analysis are quite complex under such conditions. This is attributable to the changing flow velocities and aerodynamics in both upstream and downstream sides of the Darrieus-type VAWTs (Staelens et al., 2003). Fig. 1 shows flow velocities and forces on a VAWT blade.

As the VAWT rotates with a rotational velocity ω, in a flow of free stream wind speed U_∞ , the velocity of the wind relative to the blade changes and is given by [see Danao et al. (2012); Staelens et al. (2003)]

$$\vec{W} = \vec{U}_\infty + \vec{V} \tag{3}$$

where $\vec{V} = -\omega R_{rotor}$. From Eq. (3), the relative wind velocity fluctuates from a maximum of $(\lambda+1)U_\infty$ to a minimum of $(\lambda-1)U_\infty$.

From Fig. 1(a), magnitudes of the relative velocity and angle of attack α can be expressed as [see Monteiro et al. (2013)]

$$W = \sqrt[2]{U_\infty^2+V^2} = U_\infty \sqrt[2]{1+2\lambda\ \cos\theta+\lambda^2} \tag{4}$$

$$\alpha = \tan^{-1}\left[\frac{\sin\ \theta}{\left(\frac{\omega R_{rotor}}{U_\infty}\right)+\cos\ \theta}\right], \tag{5}$$

where θ is the azimuth angle (refer to Fig. 2). From Eq. (5), the angle of attack α, also varies periodically between the positive and negative values, and it is equivalent to zero when the blade is parallel and faces into the wind at a particular azimuth angle θ

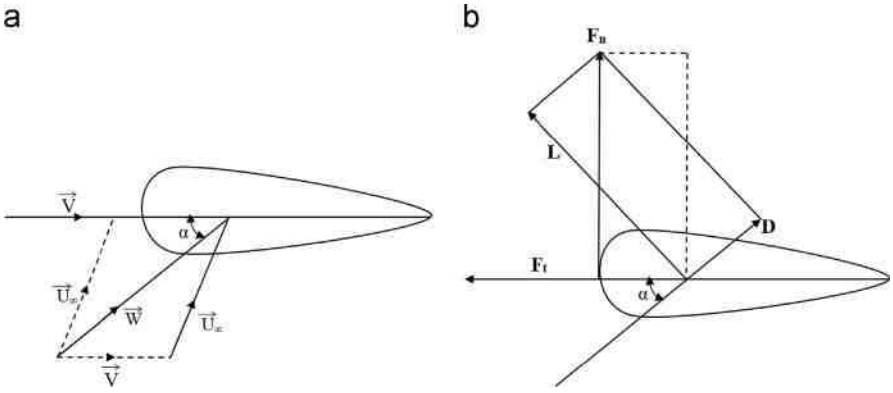

Fig. 1. Flow velocities and forces on a VAWT blade. (a) Flow velocities. (b) Blade Forces.

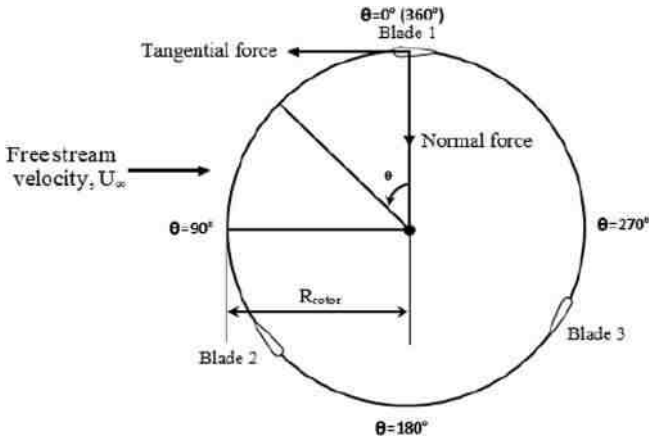

Fig. 2. Free stream wind direction, azimuth positions and orientation of blades.

(Sasson and Greenblatt, 2010; Yen and Ahmed, 2013). The relative positions of the rotor blades and azimuth positions θ, with respect to the mid-chord of blade 1 are as shown in Fig. 2.

From Eqs. (2) and (5), we can imply that, the VAWT at low blade speed ratios between 1 and 3 can experience large time-varying blade angles of attack up to $\pm 50^{\circ}$ that induce strong dynamic stall effects. As a result, this produces periodic formation and shedding of vortices that impinge on downstream blades causing poor turbine performance, as well as undesirable blade vibrations and damage (Yen and Ahmed, 2013).

The directions of the lift and drag forces and their normal and tangential components are shown in Fig. 1(b). The tangential force coefficient (C_t) is the difference between the tangential components of lift and drag forces. Similarly, the normal force coefficient (C_n) is the difference between the normal components of lift and drag forces. The normal and tangential force coefficients are related to the Lift and Drag coefficients (respectively, C_L and C_D) by

$$C_n = C_L \cos \alpha + C_D \sin \alpha; \tag{6}$$

$$C_t = C_L \sin \alpha - C_D \cos \alpha, \tag{7}$$

where α is the angle of attack (AOA).

The net tangential and normal forces can be defined as

$$F_t = C_t \tfrac{1}{2} \rho A W^2, \tag{8}$$

$$F_n = C_n \tfrac{1}{2} \rho A W^2, \tag{9}$$

where ρ is the air density and A is the VAWT projected area. The tangential and normal forces represented by Eqs. (8) and (9) are for any azimuthal position; hence, they are considered as a function of azimuth angle (Islam et al., 2008). The average tangential force (F_{ta}), on one blade can be expressed as

$$F_{ta} = \frac{1}{2\pi} \int_0^{2\pi} F_t(\theta)\, \mathrm{d}\theta. \tag{10}$$

The average Torque T_a, is expressed as [see Abdelsalam et al. (2014)]

$$T_a = F_{ta} R_{rotor} + M \tag{11}$$

where M is the average pitching moment produced on the blade (Sasson and Greenblatt, 2010), and is given as

$$M = \int_0^{2\pi} C_m \frac{1}{2} \rho W^2 A^2\, \mathrm{d}\theta. \tag{12}$$

However, the moment of Eq. (12) is not considered in our study, because both turbine blades under investigation are symmetric.

In this paper, force coefficients on a single blade of the VAWT were computed from the simulations to aid in the analysis. Instead of using standard aerodynamic definitions of the different dimensionless coefficients, the following more appropriate expressions were adopted, respectively, for lift, drag and moment coefficients [see Bottasso et al. (2014)].

$$C_l = \frac{L}{\frac{1}{2}\rho V^2 A}, \tag{13}$$

$$C_d = \frac{D}{\frac{1}{2}\rho V^2 A}, \tag{14}$$

$$C_m = \frac{T}{\frac{1}{2}\rho V^2 A R_{rotor}} \tag{15}$$

where T is the blade torque and V is the blade linear velocity as given in Eq. (3). The definition of dynamic pressure ρV^2, by use of blade linear velocity instead of the relative velocity, is intentional. For a VAWT blade, the relative velocity is constantly changing in both magnitude and incidence. Therefore, to facilitate the comparison of the force coefficients between different airfoil profiles, the use of a constant reference velocity is preferred (Danao et al., 2012).

However, from the moment coefficient Eq. (15), unlike Lift and Drag coefficients in Eqs. (13) and (14), respectively, there is an additional factor R_{rotor} which is the rotor radius for VAWT. Observe that, in both airfoil and VAWT applications, Eq. (15) remains the same, because we are getting the blade force coefficient, not the rotor coefficient. The only change is that in static airfoil studies, on the one hand coefficient of moment is normally computed about the quarter chord from the leading edge of the airfoil. On the other hand, for VAWT problems, moment coefficient is referred to from the VAWT rotation axis.

3. Methodology

3.1. Numerical set up

In Eboibi et al. (2013), Danao et al. (2012), Danao et al. (2014), Untaroiu et al. (2011), Ferreira et al. (2011), Nobile et al. (2014), the 2D CFD model has been used to represent the virtual wind tunnel to reveal and predict the aerodynamic performance and flow physics around the VAWTs. Based on these studies, it has been shown that a 2D model is sufficient in predicting the performance and aerodynamics that surround the VAWT. The contributions of blade end effects and blade-support arm junction effects are neglected but deemed acceptable since these can be considered as secondary (Danao et al., 2014).

In this study, a steady wind performance is initially analyzed over tip speed ratio of range from $\lambda = 2$ to $\lambda = 5.5$ with increments of 0.5 for constant free stream velocity U_{mean} of 11.00 m/s. This is the mean wind speed condition for Marsabit station, a rural–urban town in Eastern Kenya Kamau et al. (2010).

Choosing a suitable computational domain is a key step in correctly reproducing fluid-dynamic phenomena (Lanzafame et al., 2013). In this paper, the CFD computational domain consists of two mesh zones: the inner circular Rotor sub-grid zone and the rectangular outer zone. The inner Rotor sub-grid zone is composed of three symmetric airfoil blades rotating at a common angular velocity. The three airfoil blades are spaced equally at 120° apart as shown in Fig. 2.

Fig. 3(a) shows the main wind tunnel scale dimensions and the boundary conditions of the 2D numerical wind tunnel domain. From the wall distance study by Danao et al. (2014), the outer rectangular domain zone boundary was set to 2.4 m rotor diameter, to minimize the effect of wake development by the VAWT. The rectangular outer domain is a wind tunnel grid with the wind

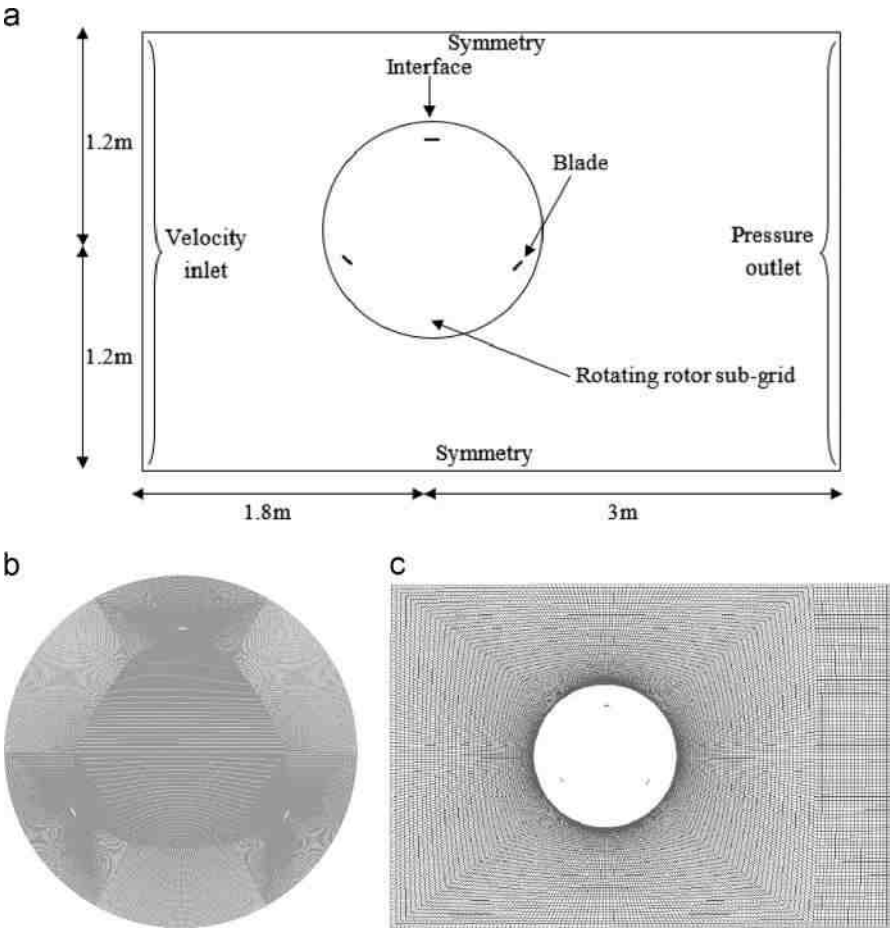

Fig. 3. An illustration of the wind tunnel Computational domain. (a) 2D numerical domain. (b) Rotating inner domain mesh. (c) Stationary outer domain mesh.

velocity inlet placed at 1.8 m rotor diameter upwind on the left side that allowed the magnitude of inlet flow (Danao et al., 2013). The right hand side is the pressure outlet boundary condition placed at 3 m rotor diameter downwind to match the experimental set up by Danao et al. (2013). This was to ensure that the wake by the VAWT was not terminated prematurely for the unsteady wind conditions under this study.

Therefore, the potential problem of computational boundaries interacting with the flow around the turbine was minimized. Since the main focus of the study is on VAWT unsteady inflow wind performance as a result of blade aerodynamic fluctuations, the preliminary tests for computational boundary have not been discussed in this paper. For full details on domain boundary location with both mesh and time step independence preliminary studies including the relevant assumptions made, the reader is referred to (and references therein Edwards et al., 2012; Danao et al., 2014; McTavish et al., 2013b; Gomez-Iradi et al., 2009).

The bottom and the top side of the domain were defined as symmetry boundary condition to represent that the 2D model was extrapolated from the midsection of the actual setup which is 3D. A wall type boundary condition was also tested, and results recorded were similar to the symmetry boundary condition. Within the rectangular outer zone is a circular hole to fit in the inner circular Rotor sub-grid. The blades were defined as no slip walls, while both interface boundary of the Rotor sub-grid and the outer rectangular wind tunnel sub-grid were set as an interface. The interface was defined by coupling the stationary domain with the rotating one.

In this simulation, the effects due to rotor support arms and torque shaft were not taken into account due to the 2D simulation dimensionality. A moving mesh was used for the rotation of the inner circular Rotor sub-grid zone in order to capture the torque generated by the three blade airfoils. The images of the adopted mesh of the computational domain is as observed in Fig. 3(b) and (c). The inner circular Rotor sub-grid zone (Fig. 3(b)) coincides exactly with the circular opening within the outer stationary rectangular zone (Fig. 3(c)). The interface of the two zones slide against each other, and have approximately the same characteristic cell size in order to obtain faster convergence (Danao et al., 2014; Raciti Castelli et al., 2011).

In this study, unsteady Reynolds-Averaged Navier-Stokes (RANS) equations are solved for the entire flow domain using commercial CFD software package ANSYS Fluent 14.5. This code uses the finite volume method to solve the governing equations for fluids. The coupled pressure-based solver was selected with a second order implicit transient formulation for improved accuracy (Makridis and Chick, 2013; Esfahanian et al., 2013). All the solution variables were solved via second order upwind discretization scheme, since most of the flow can be assumed not to be in line with the mesh (Danao et al., 2014; Makridis and Chick, 2013). The turbulence intensity of inlet flow is set to 8% with a turbulence viscosity ratio of 14. These conditions were selected to provide a matching turbulence intensity decay that was observed in VAWT experiments conducted in the wind tunnel facility based on three NACA0022 blades with chord $c=0.04$ m (Danao et al., 2013). The rotor radius R_{rotor} and the rotor blade length (blade span) L are 0.35 m and 0.6 m, respectively, giving the VAWT a solidity of $\sigma=0.34$.

The CFD software package ANSYS Fluent 14.5 was used to directly obtain the instantaneous blade Torque T_b. The obtained T_b was an average value after 9 rotations of the turbine assuring that

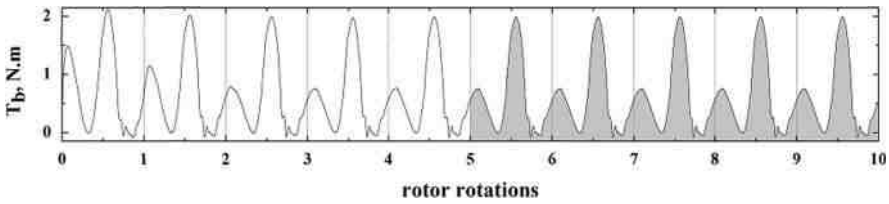

Fig. 4. 10 full rotations blade Torque, T_b, ripple.

the steady solution was reached. The irregularity in the torque peaks of upwind and downwind can be seen for the first five cycles as shown in Fig. 4. The blade torque peak values of the upwind and downwind for cycles 5 to 10 matched closely; with a marginal difference of about 0.5% between the last five cycles of the rotation. This was a reflection of mesh quality, and times step size equivalent to 1×10^{-5} s for each physical time step. It was appropriate to select time step size at the lower tip speed ratio with converged solutions so as to ensure convergence at the higher tip speed ratio was achieved (Eboibi et al., 2013; Rossetti and Pavesi, 2013).

A period corresponds to a revolution of 120° due to the three bladed rotor geometry; hence a 360° rotation was considered in all the simulations. A plot of T_b monitored through 10 rotations is as observed in Fig. 4. A shift in the torque ripple for each succeeding blade by 120° is observed for rotations where the simulation is fully converged. At the last five cycles of rotation, each 360° torque ripple of one blade match the other blades at 120° apart.

The time step convergence was monitored and the simulation was considered to have converged when residuals of all conserved variables fell below 1×10^{-5} (Raciti Castelli et al., 2011; Danao et al., 2014). The present simulations required an average of about 20 sub-iterations to make the solution converge at each physical time step. The calculations were performed on a computer having, Intel(R) Core (TM) i7-2600 CPU @3.40 GHz 3.70 GHz physical RAM of 8 GHz and Windows 8 professional 64-bit operating System. A total Central Processing Unit (CPU) time of approximately 3 days was required for each simulation.

3.2. Validation of CFD model

Appropriate CFD numerical validation solution has been conducted by Danao et al. (2012) with a pitching airfoil experiment data at a Reynolds number of 1.35×10^5. According to the authors, the dynamic interactions of a pitching airfoil with a moving fluid give closest possible validation cases versus static airfoil data in the absence of VAWTs experimental data. The results show that both fully k-ω Shear Stress Transport (SST) and the Transition SST were the most accurate models for predicting dynamic behavior compared to popular turbulence models like the one-equation Spalart–Allmaras (S–A) and the two-equation renormalisation group RNG k-ε. To assess the suitability of Danao et al. (2012) results, Danao et al. (2014) revealed that Transition SST model predicted positive CP performance closer to Particle Image Velocimetry (PIV) experimental results CP than SST k-ω model.

To check and validate the numerical model, a 2D simulation was carried out using Transition SST turbulence model. The reference parameter for the present analysis is the power coefficient (CP) plotted against the tip speed ratio (λ).

The CFD simulations with a steady incoming winds of 7 m/s and 11 m/s were tested against the experimentally derived CP by Danao et al. (2013) at different tip speed ratios from $\lambda=1.5$ to $\lambda=5$ with increments of 0.25. As can be seen from Fig. 5, the turbulent model over-predict the CP experiment starting from $\lambda=2.0$ to $\lambda=5$.

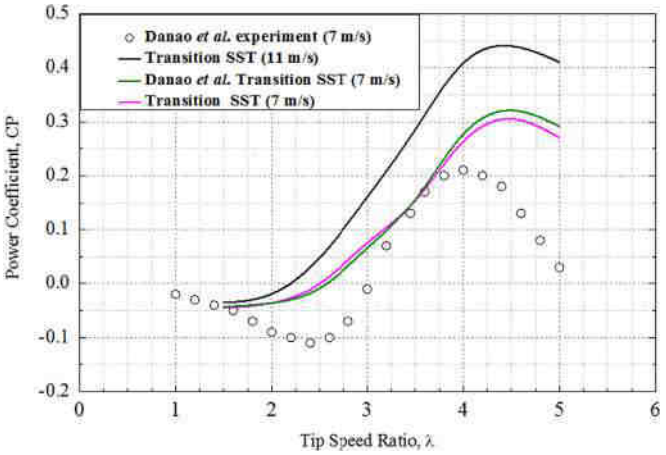

Fig. 5. Steady CP curves.

In addition, it can be observed in Fig. 5 that the Transition SST model generates maximum CP at $\lambda=4.5$ for both wind speeds, with $U_\infty=11$ m/s predicting higher CP and wider band of positive performance than $U_\infty=7$ m/s. The higher CP over-prediction at 11 m/s was expected and is attributable to wind power dependency on the cube of the wind speed (refer to Eq. (17)).

The gap in predicted CP was expected as a result of 2D model inability to account for finite blade span as well as the blade-support arm junction effects and support arm drag that are present in the actual setup (Raciti Castelli et al., 2011; Vahdati et al., 2011; Battisti et al., 2011). The Transition SST turbulence model CP over-prediction results are consistent with published work in Edwards et al. (2012), Danao et al. (2014), Raciti Castelli et al. (2011), Howell et al. (2010); Li and Calisal (2010), where 2D power coefficients were over-predicted over the entire range for λ.

As can be seen in Fig. 5, the maximum CP for the experiment is 0.21 at $\lambda=4.0$, while the study's Transition SST model maximum CP is 0.30 at $\lambda=4.5$ for steady speed of 7 m/s. The study's Transition SST results are similar to those of Danao et al. Transition SST model (Danao et al., 2014), maximum CP of 0.33, at a 7 m/s. The marginal overprediction by 0.03 at λ range of 3.5–5 in Danao et al. Transition SST model (Danao et al., 2014) could be attributed to the differences in the outlet and inlet distances by 1 m and 0.3 m, short of the 3 m and 1.8 m, respectively, to the study's wind tunnel domain (as shown in Fig. 3(a)). That means, the effect of developed wake was minimized to match wind tunnel set up conditions (Danao et al., 2013).

However, at low λ of between 2 and 3.5, the reverse marginal difference was observed in CP. This could be the result of the presence of the centre post in Danao et al. (2014) model that generates a wake, hence leading to blade interaction.

From Fig. 5, the Transition SST model traces experimental results by Danao et al. (2013) for positive performance prediction. Therefore, in this study, the Transition SST model is used for all subsequent VAWT simulations.

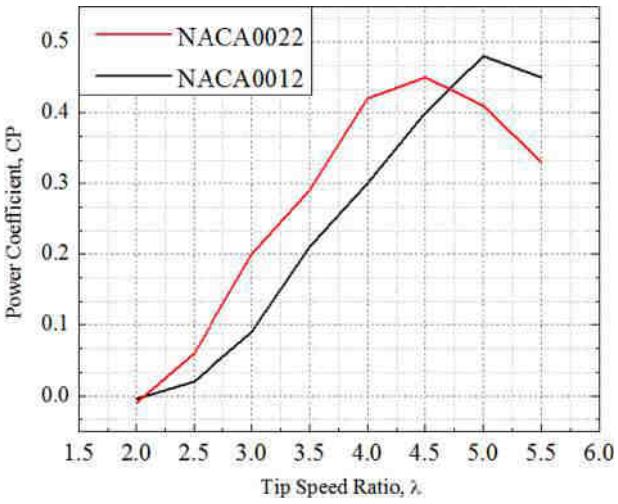

Fig. 6. Steady CP curves at 11 m/s.

4. Results and discussion

4.1. Steady wind performance

Fig. 6 shows a steady wind performance of VAWT NACA0012 and NACA0022 blade profiles, over tip speed ratio of range from $\lambda=2$ to $\lambda=5.5$ in increments of 0.5, for constant free stream velocity U_{mean} of 11.00 m/s. The thinner NACA0012 airfoil profile produces higher maximum CP than thicker NACA0022 profile. This is attributable to the lowest zero lift drag that increases maximum lift/drag ratios and the maximum values of CP obtainable. The NACA0012 profile CP curve is seen to have a sharp drop from the maximum CP on both sides, while NACA0022 profile CP curve becomes fuller with flatter top and gentler rounded drop in CP with reducing tip speed ratio.

In addition, as can be observed in Fig. 6, the maximum CP is 0.45 at optimal tip speed ratio $\lambda^*=4.5$ for NACA0022 profile, while NACA0012 generates higher maximum CP of 0.48 at $\lambda^*=5.0$. The λ^* for NACA0012 blade profile ($\lambda^*=5.0$) is 5% higher than NACA0022 blade profile ($\lambda^*=4.5$). This is as a result of higher blockage induced by the NACA0022 profile on the incoming flow-field due to its higher thickness than NACA0012 profile. Hence, the optimal value of tip speed ratio λ^* is shifted to the left of the CP-λ curve.

Using a free vortex model, Mcintosh (2009) observed similar trend in CP performance, for a family of NACA symmetric airfoils with a variation between 12% to 25% thickness. A higher stall angle was also observed to move the CP maximum to lower tip speed-ratios. This is seen as beneficial for turbines operating in a gusty environment as, for the same magnitude gust, a turbine operating at a lower tip-speed-ratio initially will experience smaller fluctuations in tip speed ratio as a result of the gust. Since the main focus of this study is on unsteady wind inflow investigation, in unsteady wind conditions, detailed explanation for steady aerodynamic performance of the VAWT can be obtained in Danao et al. (2012), McTavish et al. (2013b), Raciti Castelli et al. (2011), Sayed et al. (2012).

4.2. Unsteady wind performance

The optimized numerical model developed for the steady wind case is used in the unsteady wind simulations. Apart from the unsteady wind inflow at the velocity inlet boundary condition, the only other distinction regarding the unsteady wind model is that all three blades are monitored as opposed to one blade force monitor in the steady wind case (Danao et al., 2014).

4.2.1. Reference case

The mean wind speed $U_{mean}=11.00$ m/s with fluctuation amplitude of $U_{amp}=\pm 39\%$ (± 4.26 m/s) is selected to act as the reference to which parametric variations for both airfoil profiles can be compared. A common fluctuation frequency $f_c=1$ Hz is used as a reference for both VAWT airfoil profiles. This is as a result of studies in Scheurich (2011), Danao et al. (2014), Bertényi et al. (2010a), from which it was estimated that the highest frequency with meaningful energy content in unsteady wind environment with fluctuating wind conditions is within frequency range of ≤ 1 Hz. The rotor angular speed is a constant $\omega=149.29$ rad/s (1426 rpm), resulting into a mean tip speed ratio $\lambda_{\text{mean}}=4.75$. This is the tip speed ratio at which the steady CP-λ curves for both profiles intersect as can be seen in Fig. 6. The rotor angular speed was kept constant in order to isolate the aerodynamic effects that are introduced by the fluctuation in wind speed from the additional unsteady aerodynamic effects that will be introduced when the rotor accelerates or decelerates.

Following McIntosh et al. (2008) notation for VAWT experiencing a gust, the number of rotor rotations n_{rev} in one full cycle of the wind fluctuation can be expressed as

$$n_{\text{rev}}=\frac{\lambda_{\text{mean}}U_{mean}}{2\pi R_{\text{rotor}}f_c}, \tag{16}$$

where λ_{mean} is the mean tip speed ratio corresponding to the ω_{mean}, U_{mean} is the fluctuating mean wind speed, R_{rotor} is the rotor radius and f_c is characteristic fluctuation frequency. Therefore, in the present wind conditions, 24 full rotations of the rotor were allowed to run to capture periodic convergence each associated with one wind cycle for fluctuating mean wind speeds U_{mean} at 11.00 m/s.

Observe in Fig. 7(a) that, a simple sine wave profile for $U_{mean}=11.00$ m/s fluctuations is assumed, and the simulation is such that one wind cycle is exactly 24 rotor cycles. Yet, the simulations had to be run for 30 full rotations of the VAWT in order to have a data set that is sufficiently long to cover 24 full rotations in an entire wind cycle.

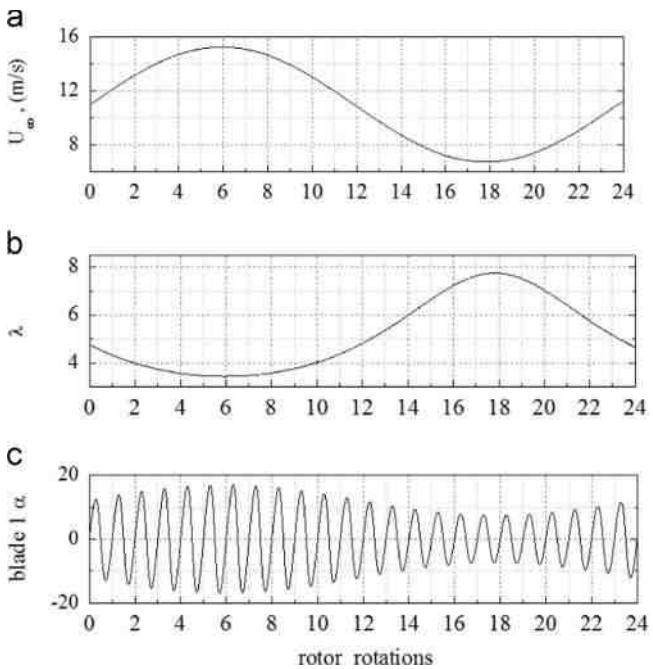

Fig. 7. One wind cycle variation of U_∞, λ and α at $U_{mean}=11.00$ m/s. (a) One wind cycle U_∞ fluctuation. (b) One wind cycle λ fluctuation. (c) One wind cycle α fluctuation.

From Eq. (2), we may conclude that an increase in U_∞ results into a decrease in λ due to their inverse relationship at constant rotational speed ω. The incoming U_∞, increases from its mean value of 11.00 m/s to the upper peak value of 15.26 m/s at the 6th rotation, with λ droppng to a minimum value of 3.42; close to the point of maximum wind speed (refer to Fig. 7(a) and (b)). The U_∞ then drops back in speed to the mean wind speed as the blade passes the 180° azimuth position. The wind speed continues to fall until it reaches the lowest trough value of 6.74 m/s (at the 18th rotation). After which it rises again in mean velocity as the blade completes one wind cycle.

At minimum U_∞, λ rises to its maximum value of 7.55 before finally dropping back to initial $\lambda_{\text{mean}}=4.75$ (see Fig. 7(b)). Observe in Fig. 7(c) that, a low α of about 7.6° is generated by blade 1 at minimum U_∞. It should be noted from Eqs. (2) and (5) that both blade profiles yield similar blade kinematics results as can be revealed in Fig. 7. Therefore, in unsteady wind conditions, the blade kinematics (of U_∞, λ and α) is independent of the blade profile thickness.

4.2.2. Blade aerodynamic loading

The effect of Unsteady winds on the power output is revealed in more detail by analyzing the aerodynamic loading on the VAWT blade profiles.

From Fig. 8(a) and (b), both blade profiles exhibit similar pattern of geometric angle of attack in both steady and unsteady wind conditions. The azimuth peaks close to 90° are observed in steady wind conditions for the variation of the angle of attack and normal aerodynamic loading in both profiles. However, the steady variation of the azimuth positions and the tangential aerodynamic loading exhibits peaks close to 60°.

In addition, observe in Fig. 8(a) and (b) that, the aerodynamic angle of attack in unsteady wind conditions shows comparable features to those observed in steady wind conditions. Both blade profiles experience maximum peak close to 90° azimuth in a single revolution. While, from Fig. 8(c)–(f), the variation of normal and tangential force coefficients differs from rotor revolution to rotor revolution when the turbine is operated in unsteady conditions. Similar results were observed by Berténi et al. (2010a) study using the free Vortex model method.

Fig. 9 shows flow visualization of vorticity profiles as the U_∞ fluctuates across one rotor revolution of the wind cycle at $U_{mean}=11.00$ m/s. Since there is no visible difference between the three blades at the same θ, stalling of one blade at different rotor cycles is monitored. This could be the result of low frequency of the wind speed cycle compared to that of the rotor cycle (Danao et al., 2014).

In Fig. 9 it can be seen that there is no visible flow separation on the blade surface for azimuth position $\theta=60°$ in both blade profiles following thin wake. This is attributable to the stagnation point staying at the trailing edge. Partial separation can be observed from $\theta=90°$ in both blade profiles with a more visible full separation stall at $\theta=130°$ for NACA0012 blade profile than NACA0022 blade profile. This can be as a result of negative normal force coefficient that the blade experiences at the region inducing persistent large scale vortex shedding as evidenced in Fig. 8(d). The vorticity flow field across both blade profiles in the downwind region shows a similar pattern of re-attachment.

4.2.3. Effect of varying blade thickness

The CFD method was used to analyze the effect of 22% and 12% thick blade profiles on VAWT CP performance under unsteady winds, and the results compared to the steady results (see Fig. 6). The cycle-averaged power coefficient CP of a turbine operating in an unsteady wind can be defined as the ratio of blade average power P_B to wind average power P_w over one wind cycle expressed as [see Nobile et al. (2014), Pourrajabian et al. (2014)]

$$CP=\frac{P_B}{P_w}=\frac{T_B\omega}{\frac{1}{2}\rho AU_\infty^3} \tag{17}$$

where T_B is the total blade torque, which is the average of the instantaneous torque of the three blades obtained by the solver (Eq. (15)). The blade average power is obtained by computing the average of the instantaneous blade power of the three blades over the entire wind cycle.

From Table 1, and contrary to the steady results in Fig. 6, the unsteady wind CP generated over one wind cycle by NACA0022 blade profile is 0.36, 19% higher than 0.29 of NACA0012 profile. Therefore, within fluctuating free stream wind conditions, thicker airfoils are desirable. This is because turbines operating at lower tip speed ratios will experience smaller fluctuations in λ during the gusts and the drop in CP is also reduced.

Fig. 10 shows the variation of blade power P_B and fluctuating wind power P_w across the wind cycle for both blade profiles at $U_{mean}=11.00$ m/s. The available power in the wind increases with rising free stream velocity U_∞ up to the maximum peak values generated within the 6th rotation (see Fig. 7(a)). Afterwards, wind power plummets to its minimum value of 131 W as U_∞ drops to lowest value of 6.74 m/s in the second half of the wind cycle. Observe in Fig. 10(a) and (b) that, the maximum peak P_w is 1524 W for both blade profiles.

In addition, from Fig. 10, we may conclude that the performance of the turbine in a fluctuating wind is a function of the tip-speed-ratio set by its controller, and follows the wind velocity variations. In Table 1, it can be seen that thinner blade profile (NACA0012) experiences higher negative cycle averaged CP deviation from the steady CP in unsteady winds than NACA0022 blade profile. A drop of about 40% from the steady maximum CP of 0.48 for NACA0012 blade profile is registered, while NACA0022 profile registers a drop of 20%. The drop from the maximum steady CP of NACA0022 is half of the NACA0012 profile. This is directly proportional to blade percentage thickness, of which NACA0022 blade turbine is approximately twice thicker than NACA0012 blade profile.

The study results are in agreement with parametric experimental studies in Mcintosh (2009) using realistic symmetric airfoil polars to aid in the understanding of VAWT operations. From the experimental results, as airfoil thickness was increased, the CP curve was seen to become fuller, with a flatter top and a more gentle, rounded drop in CP with reducing tip speed ratio. As a result, this was seen beneficial for turbines operating in a gusty environment as, for the same magnitude gust, a turbine operating at a lower tip speed ratio initially will experience smaller fluctuations in tip speed ratio as a result of the gust (Mcintosh, 2009).

4.2.4. Effect of varying mean tip speed ratio λ_{mean}

To investigate the effect of varying mean tip speed ratio, two more simulations were run at rotor angular speed $\omega=134$ rad/s (1276 rpm) and $\omega=165$ rad/s (1576 rpm) for both blade profiles, resulting in $\lambda_{\text{mean}}=4.25$ and $\lambda_{\text{mean}}=5.25$, respectively. The reference rotor angular speed is a constant 149.29 rad/s (1426 rpm) resulting into a mean tip speed ratio of $\lambda_{\text{mean}}=4.75$.

Fig. 11(a) shows the variation of λ with time for the three mean λ_{mean} cases of both blade profiles. The maximum and minimum λ for the reference case of $\lambda_{\text{mean}}=4.75$ is 8.16 and 3.35, respectively. The corresponding peak-to-peak value for the reference case is 3.81. The maximum λ value increases to 9.02 with the highest λ_{mean} at 5.25, while the minimum is now at 3.70 resulting into a peak-to-peak value of 5.32.

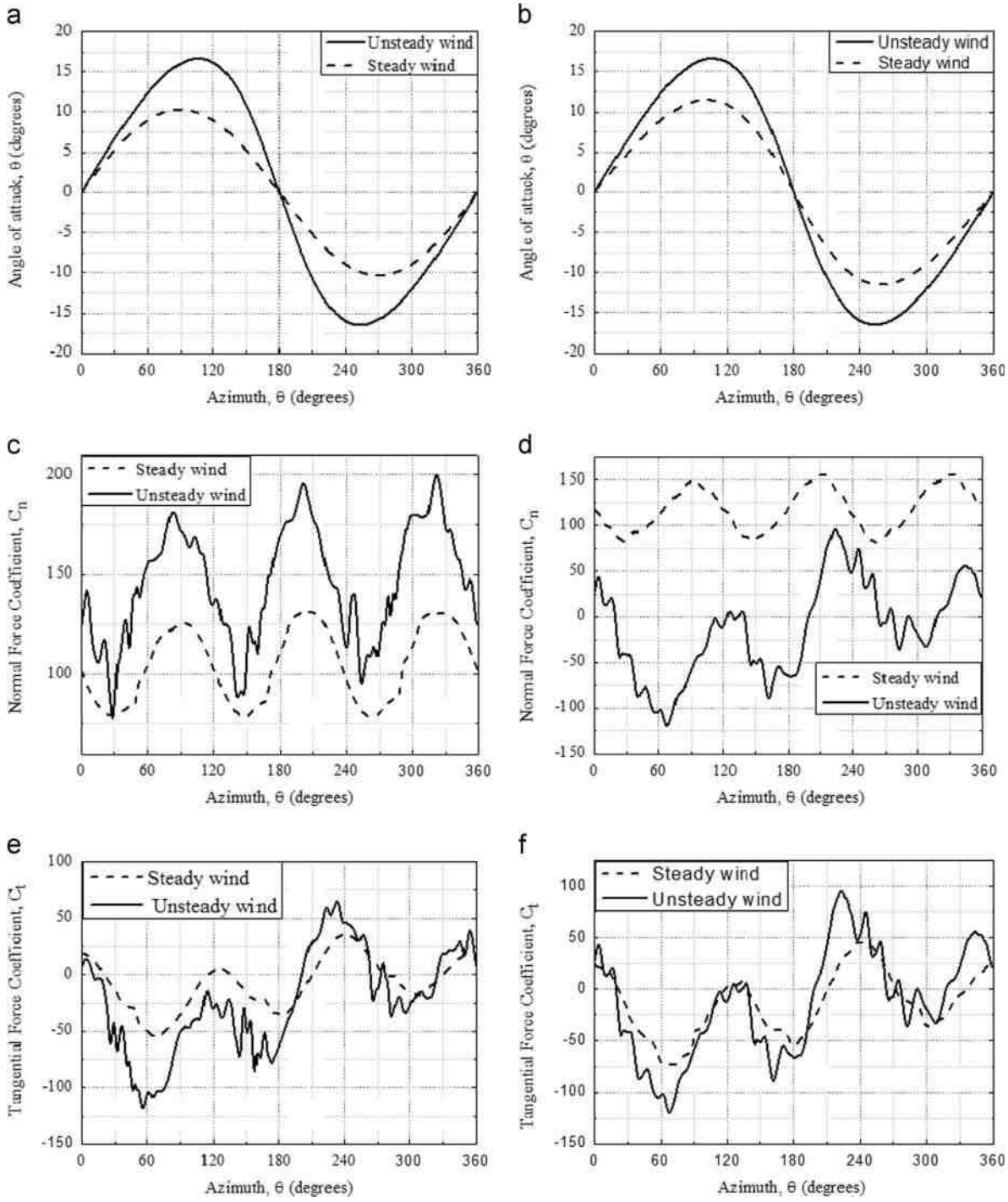

Fig. 8. Aerodynamic angle of attack and the normal and tangential force coefficients in steady and unsteady wind conditions (with $f_c = 1$ Hz at 11 m/s) during one rotor revolution. (a) NACA0022 angle of attack. (b) NACA0012 angle of attack. (c) NACA0022 Normal coefficient. (d) NACA0012 Normal coefficient. (e) NACA0022 Tangential coefficient. (f) NACA0012 Tangential coefficient.

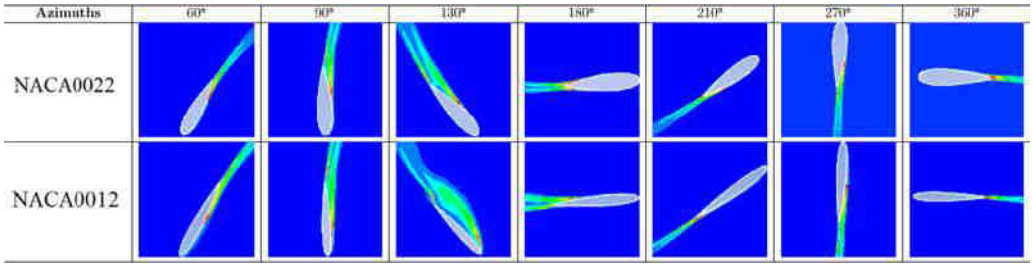

Fig. 9. Flow visualization of vorticity plots for 22% and 12% thick NACA airfoil profiles in unsteady wind conditions (with $f_c = 1$ Hz at $U_{mean} = 11.00$ m/s).

On the contrary, opposite behavior is observed at the lowest λ_{mean} at 4.25. The peak-to-peak λ value for this case is 4.30, with maximum and minimum λ seen to be 7.30 and 3.00, respectively. From the direct relationship of ω and λ in Eq. (2), at fluctuation amplitude of $U_{amp}= \pm 39\%$ (± 4.26 m/s), the peak-to-peak value increases as λ_{mean} increases. In addition, from Fig. 11(a), it can be deduced that, the VAWT model typically operates at high blade speed ratios between $\lambda=3$ and 9 in all the three λ_{mean} cases. This minimizes blade angles of attack and suppresses the onset of dynamic stall, despite the noise and safety benefits offered at low blade speed ratio operation (Yen and Ahmed, 2013).

Fig. 11(b) and (c) shows the variation of quasi-steady CP with time for both blade profiles as the wind fluctuates. The quasi-steady CP is computed from the unsteady CP using moving average smoothing method to provide useful comparative plots of CP performance for different λ_{mean} cases for both blade profiles. Smoothing filters out the fluctuating nature of the blade torque to give a single value prediction of the VAWT CP performance (Danao et al., 2014; Baker, 2010). From the figures, it can be deduced that the initial CP values for the reference case of both blade profiles are closest to the maximum steady wind CP of 0.45 and 0.48, respectively at λ^* (see Fig. 6). As a result, the NACA0022 blade profile reference starting CP is higher than that of NACA0012 blade profile.

Furthermore, both $\lambda_{mean}=4.75$ and $\lambda_{mean}=5.25$ cases record relatively higher CP at maximum λ peaks than at $\lambda_{mean}=4.25$ case for NACA0022 blade profile (refer to Fig. 11(c)). However, Fig. 11(b) shows an inverse performance at maximum λ peaks for NACA0012 blade profile.

By considering a single symmetric blade profile and initializing unsteady wind profile at $U_{mean}=7$ m/s, with a reference fluctuating amplitude of $U_{amp}= \pm 12\%$, Danao et al. (2014) observed a similar trend in the unsteady CP performance. This is attributable to low λ exhibited by very deep stall on the blades for the $\lambda_{mean}=4.25$ case that lead to negative performance (refer to Fig. 13(a) and (b)). A summary of the cycle-averaged CP for the three mean λ_{mean} cases is presented in Table 2.

Danao et al. (2013), conducted unsteady wind experimental study to investigate the influence of mean tip speed ratio λ_{mean} on the overall performance of a VAWT. The study results with a reference $\lambda_{mean}=4$, also showed a similar trend to the results of the present study as shown in Table 2. Lowering the λ_{mean} from 4.1 to 3.8 showed a large hysteresis in the unsteady CP profile that drastically affected the overall performance of the VAWT.

In addition, similar to the experimental data in Danao et al. (2013), Mcintosh (2009), it can be observed in Fig. 12 that all the quasi-steady CP curves cross the steady CP curve as the wind fluctuates for both blade thickness. As can be seen from Fig. 12(a), the NACA0012 blade profile maximum CP values are 0.45, 0.47, and 0.48 for mean λ_{mean} cases 4.25, 4.75, and 5.25, respectively. The corresponding computed cycle averaged CP (Eq. (17)) over one wind cycle are 0.25, 0.29, and 0.30, respectively (see Table 2). The NACA0012 profile maximum unsteady CP for the case when $\lambda_{mean}=5.25$ is consistent with the maximum CP value in steady wind conditions of 0.48 as can be observed from Fig. 6. Maximum CP for λ_{mean} cases when $\lambda_{mean}=4.75$ and $\lambda_{mean}=4.25$ marginally drops from the steady maximum peak by 2% and 6.25%, respectively.

The maximum CP values for NACA0022 blade profile are 0.45, 0.49, and 0.52 for mean λ_{mean} cases 4.25, 4.75, and 5.25, respectively (see Fig. 12(b)). The corresponding cycle-averaged CP, defined as the ratio of the mean blade power P_B to the mean wind power P_w over one wind cycle, are 0.30, 0.36, and 0.36, respectively (see Table 2). For the lowest λ_{mean} case when $\lambda_{mean}=4.25$, maximum CP is 0.45 at $\lambda=4.2$, and is consistent with the maximum steady CP at optimal tip-speed-ratio λ^* (refer to Fig. 6). This behavior contrasts with NACA0012 VAWT unsteady maximum CP, where higher mean λ_{mean} case when $\lambda_{mean}=5.25$

Table 1
Cycle-averaged CP for NACA0022 and NACA0012 profiles.

Blade profile	U_{mean} (m/s)	U_{amp} (m/s)	CP		f_c (Hz)	Mean λ_{mean}
			CP_{steady}	$CP_{unsteady}$		
NACA0022	11.00	4.26	0.45	0.36	1.00	4.75
NACA0012	11.00	4.26	0.48	0.29	1.00	4.75

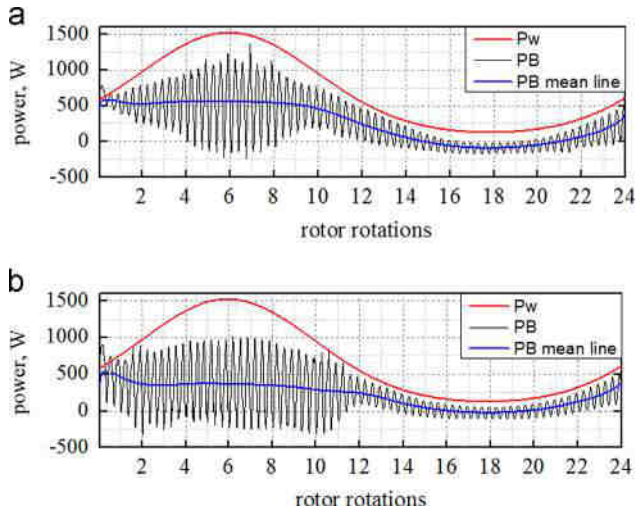

Fig. 10. One wind cycle (P_B, P_w) of NACA0022 and NACA0012 at $U_{mean}=11.00$ m/s. (a) NACA0022 blade profile. (b) NACA0012 blade profile.

Table 2
Wind cycle-averaged CP at different λ_{mean}.

Mean tip speed ratio (λ_{mean})	4.25	4.75	5.25
Cycle averaged CP (NACA0012 profile)	0.25	0.29	0.30
Cycle averaged CP (NACA0022 profile)	0.30	0.36	0.36

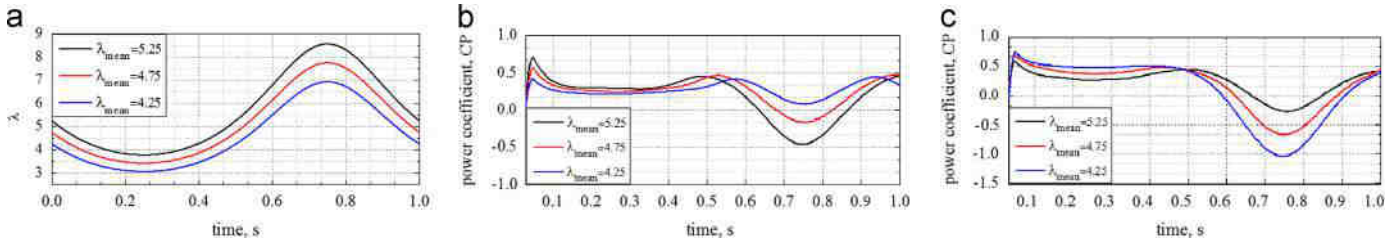

Fig. 11. (a) Wind cycle λ fluctuation. (b, c) Quasi-steady CP for different λ_{mean} cases. (b) NACA0012 CP vs. time. (c) NACA0022 CP vs. time.

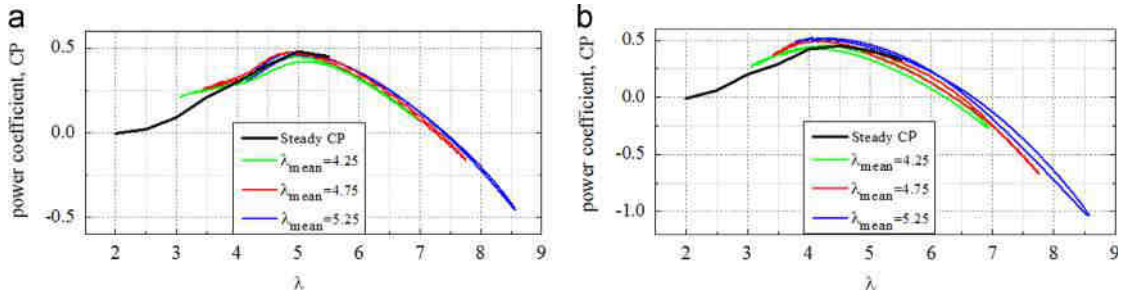

Fig. 12. Quasi-steady VAWT CP performance for different λ_{mean} cases. (a) NACA0012 profile CP vs. λ. (b) NACA0022 profile CP vs. λ.

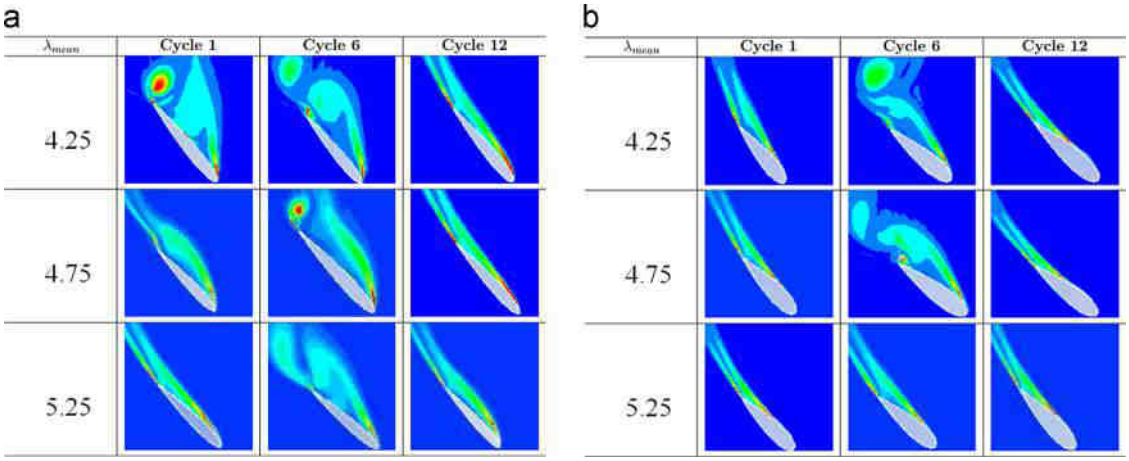

Fig. 13. Selected rotor cycles flow visualizations of vorticity plots for NACA0012 and NACA0022 profiles in the first half wind cycle showing effects of varying λ_{mean} at $\theta=130^{\circ}$. (a) NACA0012 profile vorticity plots. (b) NACA0022 profile vorticity plots.

(at $\lambda=4.9$), matches the maximum steady wind CP of 0.48. From Fig. 12(b), maximum CP for mean λ_{mean} cases of 4.75 and 5.25 reveals positive deviations above the steady optimal tip speed ratio λ^* CP of 0.45 by 9% and 16%, respectively.

The NACA0022 profile maximum CP peaks for mean λ_{mean} cases of 4.25, 4.75, and 5.25 occur at relatively lower tip speed ratios of 4.3, 4.1, and 4.2 than NACA0012 profile's maximum CP at λ of 5.0, 5.1, and 4.9, respectively. As a result, the thinnest airfoil (NACA0012) displays the highest maximum CP, likely to be due to the lowest zero lift drag.

From Fig. 12(b), as airfoil thickness is doubled, the CP curve is seen to become fuller, with a flatter top and a more gentle, rounded drop in CP with reducing tip-speed ratio. This is seen as beneficial for turbines operating in a unsteady wind environment. That means, wind turbines with thicker airfoils operating at a lower tip-speed-ratio initially will experience smaller fluctuations in tip-speed-ratio as a result of a fluctuating free-stream.

Fig. 13 shows flow visualization of vorticity plots for NACA0012 and NACA0022 blade profiles in the first half of the wind cycle for selected rotor cycles, as U_{∞} rises from 11 m/s to 15.26 m/s and then back to 11 m/s at the end of the 12th rotation.

All images are for azimuth position at $\theta=130^{\circ}$ as can be seen in Fig. 13(a) and (b). This azimuth position is selected for flow analysis as a result of characteristic full separation revealed in Fig. 10. From Fig. 13(a) and (b), deep stall is exhibited on both blade profiles for the $\lambda_{mean}=4.25$ case. The reference case of $\lambda_{mean}=4.75$ shows significantly shallower stall than the $\lambda_{mean}=4.25$ case for both profiles, with stall induced by trailing edge separation and a much thinner wake (see Fig. 13(a) and (b)).

Shallowest stall is observed by the third case for $\lambda_{mean}=5.25$ with all NACA0022 blade profile's cycles experiencing trailing edge separation extending only up to the mid-chord. However, at this case, the NACA0012 blade profile produces a relatively thicker trailing wake, with a visible ripple in the tail. As a result, a lower cycle averaged CP of 0.30 for NACA0012 blade profile is recorded than 0.36 of NACA0022 profile (see Table 2).

4.2.5. *Effect of varying the fluctuation frequency f_c*

To investigate the effects of varying fluctuation frequencies f_c, two more simulation were run at $f_c=0.5$ Hz and $f_c=2$ Hz and the results compared to the reference case of $f_c=1$ Hz for both VAWT blade profiles. Fig. 14(a) shows the variation of tip speed ratio λ with time for the f_c cases of 0.5 Hz, 1 Hz, and 2 Hz. From the λ plots, it can be observed that the λ variations of the three f_c cases have same maximum of 7.75 and minimum of 3.42. Danao et al. (2014) and Scheurich (2011) observed a similar trend in the λ variations with time. As also observed by Danao et al. (2014), increase in f_c compresses the plots laterally resulting in shorter periods (refer to Fig. 14(a)).

From Fig. 14(b), the quasi-steady maximum CP of the NACA0012 VAWT changes in decreasing values of 0.712, 0.562, and 0.504 for $f_c=0.5$ Hz, 1 Hz, and 2 Hz, respectively. The minimum CP of the reference case ($f_c=1$ Hz) is -0.163, while the case with $f_c=0.5$ Hz shows a drop of the minimum to -0.162 and with $f_c=2$ Hz to -0.101. When $f_c=0.5$, the cycle-averaged CP is 0.28 which changes to 0.29 for both $f_c=1$ Hz and $f_c=2$ Hz cases (refer to Table 3).

Unlike NACA0012 VAWT profile, at points within the wind cycle where $U_{\infty}=11$ m/s (initial, 12th and 24th rotor cycles), the NACA0022 profile predicted CP for the three f_c cases are within the 0.434–0.407 range. The NACA0022 profile quasi-steady maximum CP for f_c cases when $f_c=0.5$ Hz, 1 Hz, and 2 Hz are 0.712, 0.692, and 0.646, respectively (see Fig. 15(b)). The minimum CP of the reference case is -0.669, while $f_c=0.5$ Hz and $f_c=2$ Hz cases

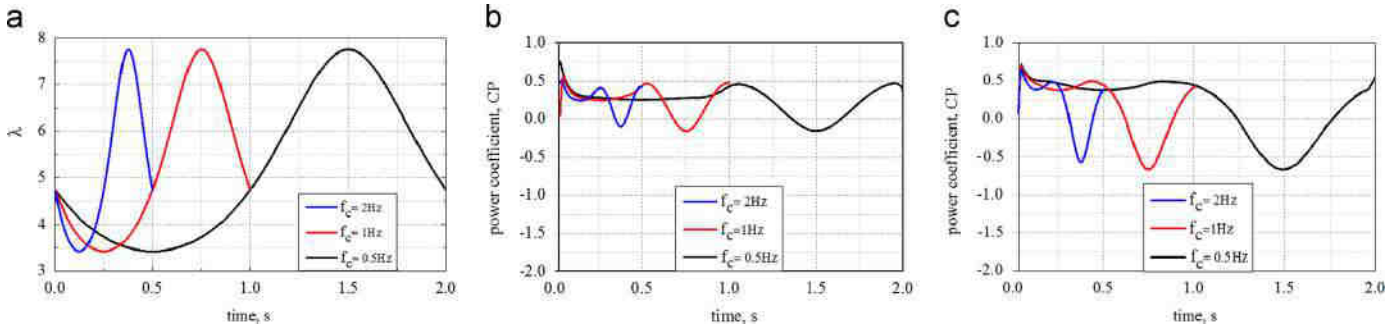

Fig. 14. (a) Wind cycle f_c fluctuation. (b,c) Quasi-steady CP for three fluctuating f_c cases. (b) NACA0012 CP vs. time. (c) NACA0022 CP vs. time.

Table 3
Wind cycle-averaged CP at different fluctuation frequencies f_c.

Fluctuation frequency (f_c)	0.5	1	2
Cycle averaged CP (NACA0012 profile)	0.28	0.29	0.29
Cycle averaged CP (NACA0022 profile)	0.35	0.36	0.36

shows minimum of −0.668 and −0.571, respectively. As can be seen in Table 3, these changes are considered to be negligible as the cycle-averaged CP marginally changes from 0.35 when f_c=0.5 Hz to 0.36 for both f_c=1 Hz and f_c=2 Hz cases.

Fig. 15 shows *CP-λ* plots of both VAWT blade profiles as the wind fluctuates for the three f_c cases. The quasi-steady CP plots for the three f_c cases have very little deviation from the reference case for both blade profiles in the high λ region. From Fig. 15(a) and (b), the unsteady CP of three f_c cases generally fall within the limits of the steady CP performance band.

The results are in agreement with the study by Danao et al. (2014), where different fluctuation frequencies were also tested and compared to the reference case f_c=0.5 Hz. At points within the wind cycle with fluctuating speed U_∞ of 7 m/s, the NACA0022 VAWT profile CP prediction for the three f_c cases of f_c=0.5 Hz, 1 Hz, and 2 Hz, were within the 0.32–0.33 range. According to the authors, the differences in CP are insignificant and can be considered negligible within the test parameters under investigation.

Using Vorticity transport model, Scheurich and Brown (2013) conducted a study on the effects of fluctuation frequency for fluctuation amplitudes of ±10% and ±30%. Two f_c were tested, a low of 0.1 Hz and a high f_c of 1 Hz for each fluctuation amplitude. Similar to the present study, their results show that the unsteady CP of both f_c cases generally fall within the limits of the steady CP performance band. Cycle-averaged CP increased by less than 2% when f_c changed from 0.1 Hz to 1 Hz. Overall performance degradation was observed when fluctuation amplitudes were high (±30%), while at a lower U_{amp} of ±10%, the cycle-averaged CP change was even smaller and less than 1% for the same f_c change from 0.1 Hz to 1 Hz.

Furthermore, at very low fluctuation frequency range, McIntosh et al. (2008) presented increased performance as f_c rose from 0.05 Hz to 0.5 Hz. The results are contrary to the present study at higher fluctuation frequencies from 1 Hz to 2 Hz, where marginal improvement in VAWT performance can be observed (refer to Table 3). Although there is no control as to what frequencies is expected in the actual field, from both the studies, there is the choice of not putting effort to extracting the energy at higher frequencies (> 1 Hz) since it is below 10% of the total energy spectrum (Scheurich, 2011; Danao et al., 2014; Bertényi et al., 2010a; Bertenyi et al., 2010b).

The effects of different fluctuating frequencies on a VAWT subjected to unsteady wind with U_{mean}=6.64 m/s, U_{amp}=±50% and λ_{mean}=4, were studied by Danao et al. (2012). In spite of increased available power, the VAWT performance degraded over one wind cycle on all unsteady wind f_c cases. In the present work, a 40% and 20% drop in cycle-averaged CP is obtained for conditions when f_c=1 Hz and U_{amp}=±39%, for 12% and 22% thick VAWT profiles, respectively. Danao et al. (2012) data showed a 75% drop in cycle-averaged CP when conditions were f_c=1.16 Hz and U_{amp}=±50%, thus agreeing with the results of the present work. The low percentage drop in CP by 22% thick airfoil of the present work is seen as beneficial to the VAWT power performance in unsteady gusty environment.

4.2.6. *Effect of varying the fluctuation amplitude U_{amp}*

The variations in U_{amp} were investigated by sinusoidally oscillating both the VAWT blades at U_{amp}=±10% (±1.1 m/s) and U_{amp}=±50% (±5.5 m/s) conditions, and compared to the reference case at U_{amp}=±39% (±4.26 m/s). Fig. 16(a) shows the variations of tip speed ratio λ with time for the U_{amp} cases of ±50%, ±39%, and ±10% for both blade profiles. From the figure, the corresponding peak-to-peak λ variations are 6.33, 4.33, and 0.96, respectively. The increase in peak-to-peak value as U_{amp} increases at a common angular velocity ω=149.29 rad/s was expected due the expanding limits of U_{amp} (Danao et al., 2014).

Fig. 16(b) and (c) shows the variation of quasi-steady CP with time as the wind fluctuates in all the three U_{amp} cases for both blade profiles. At the points of extreme U_∞ value, at the quarter cycle (t=0.25 s) and the three quarter cycle (t=0.75 s), a trough in CP curve is obtained for both VAWT profiles. From Fig. 16(b), the CP of the VAWT NACA0012 profile at the quarter cycle falls from 0.34 to 0.24, then to 0.18 with increasing U_{amp} from 10% to 39%, then to 50%. Increasing negative U_{amp} from −10% to −39%, then to −50% causes more severe drop in CP at the three quarter cycle from 0.45 to −0.16, then to −1.03, respectively.

The variation of the CP of the NACA0022 profile versus time for VAWT is similar to that of NACA0012 profile, where high amplitudes reveals larger deterioration of performance from steady CP than small amplitudes of fluctuation. From Fig. 16(c), the CP of the NACA0022 profile drops from 0.47 to 0.37, then to 0.33 (at the quarter cycle), and from 0.35 to −0.66, then to −1.86 (at the three quarter cycle) as U_{amp} fluctuates from 10% to 39%, then to 50%, respectively. As a result, in one wind cycle, increased airfoil thickness is seen as beneficial to the turbine power curves in unsteady wind environment. The large fluctuation amplitude has a detrimental effect on the VAWT operation due to the non-linear inverse relationship between U_∞ and λ (see Fig. 7(a) and (b)). Observe in Fig. 16(b) and (c) that, the CP at the start, middle, and end of the wind cycle is common in all the three U_{amp} cases for both VAWT profiles. A summary of NACA0012 and NACA0022 VAWT profiles cycle-averaged CP is presented in Table 4.

The numerical results in Table 4 are consistent to the previous experimental results in Danao et al. (2013) where the overall cycle CP was reduced when the VAWT was increased from U_{amp}=±7%

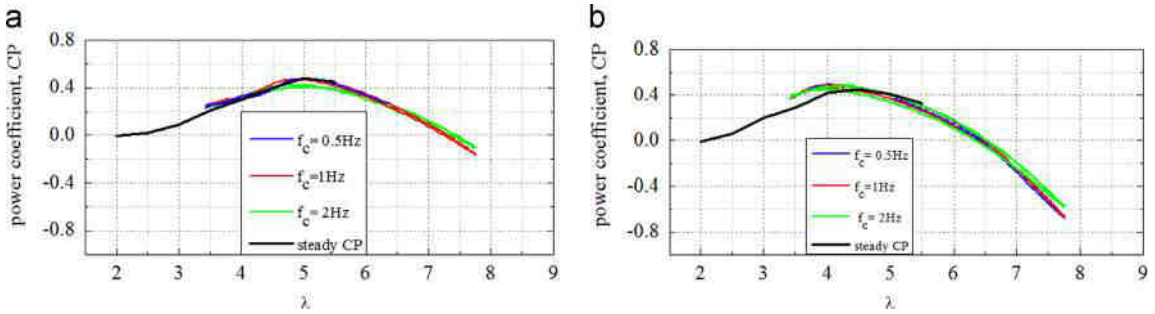

Fig. 15. Quasi-steady VAWT CP performance for different λ_{mean} cases. (a) NACA0012 profile CP vs. λ. (b) NACA0022 profile CP vs. λ.

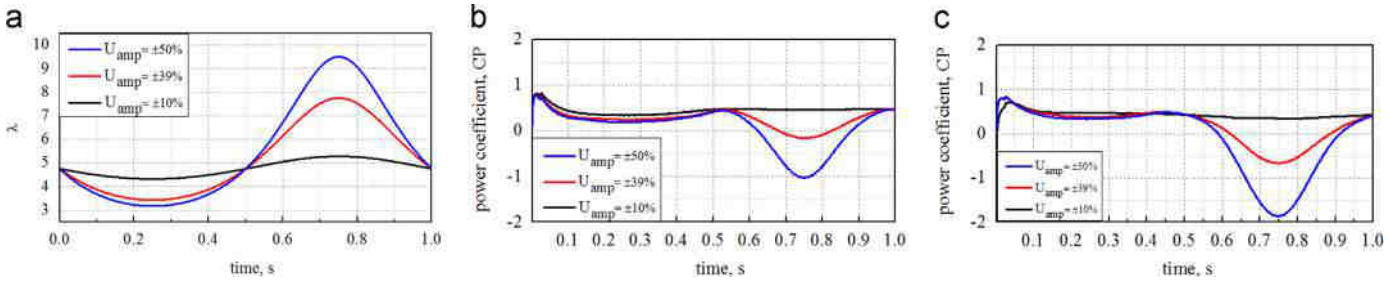

Fig. 16. (a) Wind cycle U_{amp} fluctuation. (b, c) Quasi-steady CP for three fluctuating U_{amp} cases. (b) NACA0012 CP vs. time. (c) NACA0022 CP vs. time.

Table 4
Wind cycle-averaged CP at different fluctuation amplitudes U_{amp}.

Fluctuation amplitude (U_{amp})	10%	39%	50%
Cycle averaged CP (NACA0012 profile)	0.42	0.29	0.23
Cycle averaged CP (NACA0022 profile)	0.43	0.36	0.32

to $\pm$12%, for both mean tip speed ratios at λ_{mean}=4.1 and 3.8. In addition, Kooiman and Tullis (2010) determined in their field tests that fluctuation amplitude has a linear effect on the performance of the VAWT where $U_{amp}=\pm$15% reduced performance by 3.6% from ideal wind conditions.

Fig. 17(a) and (b) shows stalling of one blade at different rotor cycles within the first half of the wind cycle at θ=130° for NACA0012 and NACA0022 profiles, respectively. From the figures, it can be observed that, partial stall is exhibited on both blade profiles for the U_{amp}=10% case in all rotor cycles following thin wake. As a result, the NACA0012 profile T_b for the three cycles reveals a marginal deviation, as shown in Fig. 18(a), where it is 1.09 Nm for cycle 1, 0.59 Nm for cycle 6, and 0.61 Nm for cycle 12. Additionally, from Fig. 18(b), the NACA0022 profile registers a relatively larger T_b of 1.16 Nm for cycle 1, 0.80 Nm for cycle 6, and 0.66 Nm for cycle 12. The large positive torque is attributable to the stagnation point staying at the trailing edge.

Partial separation can be observed at a reference case ($U_{amp}=\pm$39%) in both blade profiles across the three rotor cycles with visible full separation stall exhibited within cycle 6 (see Fig. 17(a) and (b)). The large positive T_b values evident on the upwind side in Fig. 18(c) and (d) may be attributed to the unperturbed wind and α near static stall that the blade experiences.

The last case, with largest fluctuation amplitude at U_{amp}=50%, shows deep stalling at cycle 6 (refer to Fig. 17(a) and (b)) associated with significant negative torque that the blade exhibits in cycle 6 (see Fig. 18(e) and (f)). Observe in Fig. 18(b), (d), and (f) that, NACA0022 profile T_b is largely positive throughout the upwind side with notably high values produced from θ=60° to θ=130° for U_{amp}=39% and U_{amp}=50%. The stall within this azimuth range is relatively shallow, and only becomes significant after θ=130°, where low torque is generated until the end of the upwind side. Generally, during upwind, the flow is more attached to the surface for the 22% blade thick airfoil than the 12% blade thick airfoil within a fluctuating free-stream.

The large regions of negative torque and huge visible fluctuations in Fig. 18 agree with deep stall and large flow separation of vortex shedding as shown in Fig. 17(a) and (b). The negative torque performance is a consequence of very steep α (refer to Fig. 7(c)) that the blade experiences at the regions inducing persistent large scale vortex shedding.

The results are consistent with the previous work by Danao et al. (2014) and Scheurich and Brown (2013), conducted to investigate the influence of fluctuation amplitude on the overall performance of VAWT scale. Danao et al. (2014) in their investigation run two simulations at $U_{amp}=\pm$7% ($\pm$0.49 m/s) and $U_{amp}=\pm$30% ($\pm$0.21 m/s), and compared the CP results to the reference case of $U_{amp}=\pm$12% ($\pm$0.84 m/s). Similarly, large drop in performance was observed at high fluctuation amplitude of $U_{amp}=\pm$30% than smallest fluctuation amplitude at $U_{amp}=\pm$7%. Scheurich and Brown (2013) observed that the width of the λ range was wider for the $U_{amp}=\pm$30% case than the $U_{amp}=\pm$10 % case. The VAWT cycle averaged CP dropped to 92% of the ideal steady CP for $U_{amp}=\pm$30%, while a drop to 99% of the ideal steady CP was registered for $U_{amp}=\pm$10%.

5. Conclusion

A numerical method has been presented to investigate the influence of operating conditions on VAWT of NACA00XX symmetric airfoils with 12% and 22% thickness in unsteady wind condition. The Computational Fluid Dynamics numerical method was used to analyze the aerodynamic performance and physics of flow of VAWT.

All the unsteady wind CP variation cross the steady CP curve as the wind fluctuates for both blade thickness. The unsteady wind CP generated over one wind cycle by NACA0022 blade profile was 0.36, 19% higher than 0.29 of NACA0012 profile. A drop of about 40% from the steady maximum CP of 0.48 for NACA0012 blade profile was registered, while NACA0022 profile registered a drop of 20%.

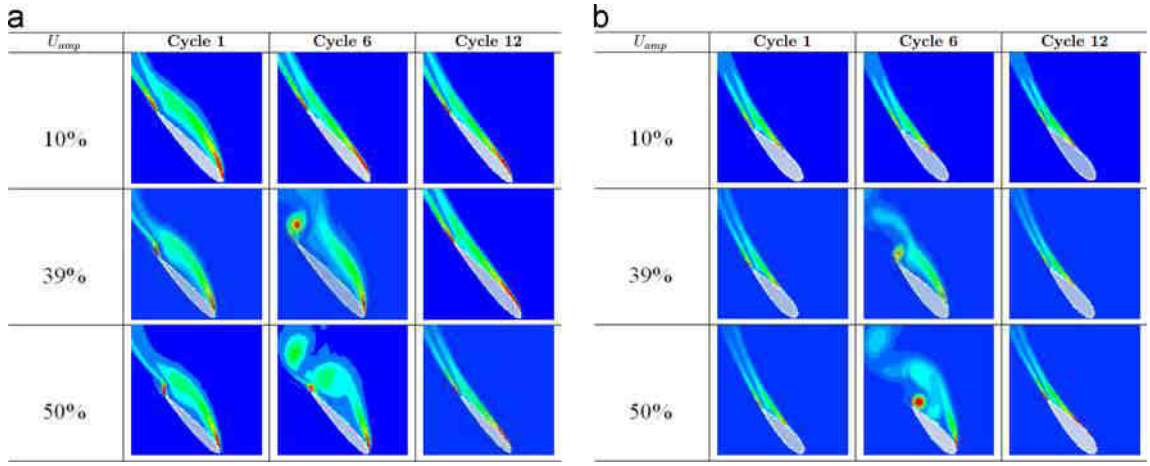

Fig. 17. Selected rotor cycles flow visualizations of vorticity plots for NACA0012 and NACA0022 profiles in the first half wind cycle showing effects of varying U_{amp} at $\theta=130^{\circ}$. (a) NACA0012 profile vorticity plots. (b) NACA0022 profile vorticity plots.

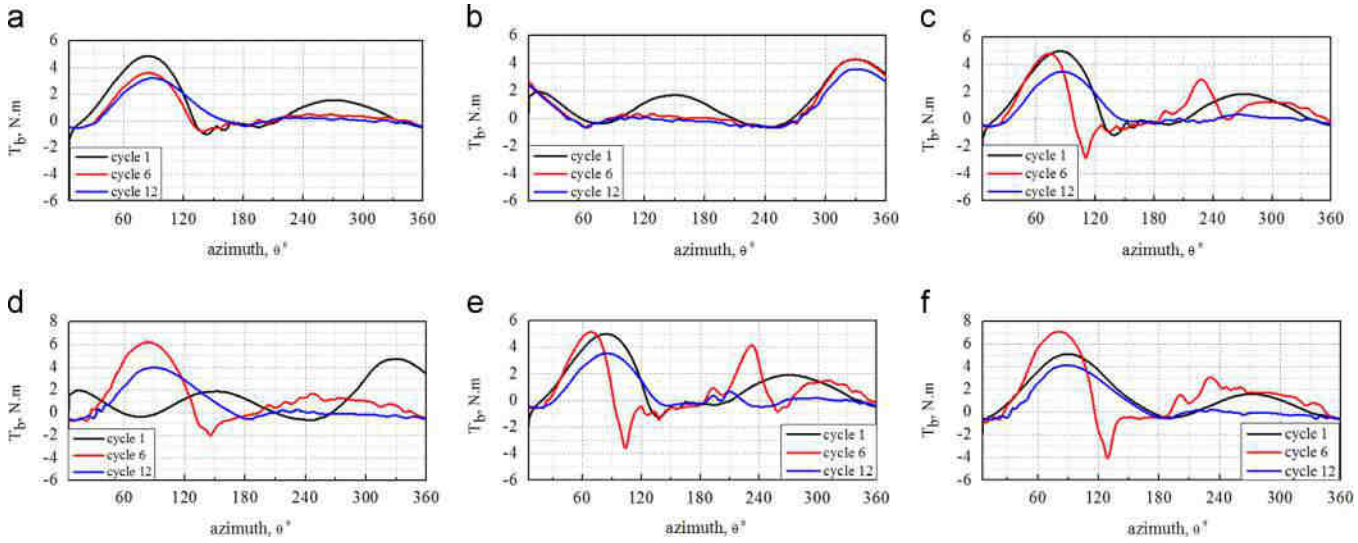

Fig. 18. Blade torque T_b for cycles 1, 6, and 12 of different U_{amp} cases. (a) NACA0012($U_{amp}=10\%$). (b) NACA0022($U_{amp}=10\%$). (c) NACA0012($U_{amp}=39\%$). (d) NACA0022 ($U_{amp}=39\%$). (e) NACA0012($U_{amp}=50\%$). (f) NACA0022($U_{amp}=50\%$).

The three unsteady wind simulations performed to investigate the effect of varying λ_{mean} have shown that the quasi-steady CP curves cross the steady CP curve for both blade thickness. The 12% blade thick cycle averaged CP computed over one wind cycle were 0.25, 0.29, and 0.30 for mean λ_{mean} cases 4.25, 4.75, and 5.25, respectively; while that for 22% blade thick were 0.35, 0.36, and 0.36, respectively. The VAWT NACA0022 profile maximum CP for mean λ_{mean} cases of 4.75 and 5.25 revealed positive deviations above the steady maximum CP of 0.45 by 9% and 16%, respectively. However, λ_{mean} cases of 4.75 and 4.25 for VAWT NACA0012 profile marginally dropped from the steady maximum CP by 2% and 6.25%, respectively.

The effects of varying frequency of fluctuation were studied by conducting three unsteady wind simulations. Thicker VAWT blade cycle-averaged CP marginally changed from 0.35 when $f_c=0.5$ Hz to 0.36 for both 1 Hz and 2 Hz cases, while thinner blade changed from cycle-averaged CP of 0.28 when $f_c=0.5$ to 0.29 for both $f_c=1$ Hz and $f_c=2$ Hz cases, respectively.

Different amplitudes of fluctuation were also tested at $U_{amp}=\pm 10\%$ and $U_{amp}=\pm 50\%$, and compared to the reference of $\pm 39\%$. The 22% blade thick cycle averaged CP computed over one wind cycle were 0.43, 0.36, and 0.32, while 12% blade thick CP were 0.42, 0.29, and 0.23, for U_{amp} cases $\pm 10\%$, $\pm 39\%$, and $\pm 50\%$, respectively.

The results derived in the numerical analysis are therefore summarized as follows:

- In unsteady wind environment, the unsteady wind CP generated over one wind cycle by NACA0022 blade profile was higher than that of NACA0012 blade profile. Hence, within fluctuating free-stream wind conditions, thicker airfoils are desirable.
- Overall maximum unsteady wind CP of VAWT with thicker blades reveals positive deviations if λ is slightly higher than optimal tip speed ratio λ^* of steady peak CP, while thinner blades maximum CP marginally drops from the steady maximum CP for the same λ range.
- Higher frequencies (>1 Hz) of fluctuation marginally improve the unsteady wind performance of both thinner and thicker VAWT blade profiles operating in periodically fluctuating wind conditions.
- High fluctuation amplitudes ($>\pm 10\%$) reveals overall performance degradation on both VAWT blade profiles, while a slight improvement is registered if the amplitude of fluctuation is small ($<\pm 10\%$).

The findings lend substantially to our understanding of both the kinematic and aerodynamic behavior on VAWT scale blades

operating in unsteady wind condition, and the flow physics that causes the behavior. The results from the study will hopefully be of importance to the wind industries and industrial aerodynamics applications that require designs for wind turbine blades, reflecting realistic unsteady wind operating conditions.

Acknowledgments

This research work was supported in part by the Institute of Dynamics and Control of Spacecrafts, School of Astronautics, through Harbin Institute of Technology; and the Chinese Scholarship Council, through P.R. China Government in collaboration with the Kenyan Government.

References

Abdelsalam, A.M., Boopathi, K., Gomathinayagam, S., Hari Krishnan Kumar, S., Ramalingam, V., 2014. Experimental and numerical studies on the wake behavior of a horizontal axis wind turbine. J. Wind Eng. Ind. Aerodyn. 128, 54–65.

Aslam Bhutta, M.M., Hayat, N., Farooq, A.U., Ali, Z., Jamil, S.R., Hussain, Z., 2012. Vertical axis wind turbine—a review of various configurations and design techniques. Renew. Sustain. Energy Rev. 16, 1926–1939.

Baker, C., 2010. The simulation of unsteady aerodynamic cross wind forces on trains. J. Wind Eng. Ind. Aerodyn. 98, 88–99.

Battisti, L., Dossena, V., Persico, G., Zanne, L., Dell Anna, S., Paradiso, B., 2011. Aerodynamic measurements on a vertical axis wind turbine in a large scale wind tunnel. J. Energy Resources Technol. 133, 031201.

Bedon, G., Castelli, M.R., Benini, E., 2013. Optimization of a darrieus vertical-axis wind turbine using blade element momentum theory and evolutionary algorithm. Renew. Energy 59, 184–192.

Bedon, G., Castelli, M.R., Benini, E., 2014. Optimal spanwise chord and thickness distribution for a troposkien darrieus wind turbine. J. Wind Eng. Ind. Aerodyn. 125, 13–21.

Berténvi, T., Wickins, C., McIntosh, S., 2010. Enhanced energy capture through gust-tracking in the urban wind environment. In: Forty-eighth AIAA Aerospace Sciences Meeting, Orlando, Florida, USA.

Bertenyi, T., Wickins, C., McIntosh, S., 2010. Enhanced energy capture through gust-tracking in the urban wind environment. In: Forty-eighth AIAA Aerospace Sciences Meeting including the New Horizons Forum and Aerospace Exposition.

Bottasso, C.L., Campagnolo, F., Petrović, V., 2014. Wind tunnel testing of scaled wind turbine models: beyond aerodynamics. J. Wind Eng. Ind. Aerodyn. 127, 11–28.

Burton, T., Jenkins, N., Sharpe, D., Bossanyi, E., 2011. Wind Energy Handbook. John Wiley & Sons; Chichester, West Sussex.

Consul, C., Willden, R., Ferrer, E., McCulloch, M., 2009. Influence of solidity on the performance of a cross-flow turbine. In: Eighth European Wave and Tidal Energy Conference. Uppsala, Sweden, Uppsala.

Danao, L.A., Qin, N., Howell, R., 2012. A numerical study of blade thickness and camber effects on vertical axis wind turbines. Proceed. Inst. Mech. Eng. A: J. Power Energy 226, 867–881.

Danao, L.A., Eboibi, O., Howell, R., 2013. An experimental investigation into the influence of unsteady wind on the performance of a vertical axis wind turbine. Appl. Energy 107, 403–411.

Danao, L.A., Edwards, J., Eboibi, O., Howell, R., 2014. A numerical investigation into the influence of unsteady wind on the performance and aerodynamics of a vertical axis wind turbine. Appl. Energy 116, 111–124.

Eboibi, O., Howell, L.A.D.R., Edwards, J.M., 2013. A numerical study of the influence of blade profile and solidity on the performance of vertical axis wind turbines. In: Fifty-first AIAA Aerospace Sciences Meeting including the New Horizons Forum and Aerospace Exposition (2013).

Edwards, J.M., Danao, L.A., Howell, R.J., 2012. Novel experimental power curve determination and computational methods for the performance analysis of vertical axis wind turbines. J. Sol. Energy Eng. 134, 031008.

Esfahanian, V., Pour, A.S., Harsini, I., Haghani, A., Pasandeh, R., Shahbazi, A., Ahmadi, G., 2013. Numerical analysis of flow field around {NREL} phase {II} wind turbine by a hybrid cfd/bem method. J. Wind Eng. Ind. Aerodyn. 120, 29–36.

Ferreira, C.J.S., Scarano, F., van Bussel, G.J., van Kuik, G.A., 2011. On the use of velocity data for load estimation of a vawt in dynamic stall. J. Sol. Energy Eng. 133, 011006.

Gomez-Iradi, S., Steijl, R., Barakos, G., 2009. Development and validation of a cfd technique for the aerodynamic analysis of hawt. J. Sol. Energy Eng. 131, 031009.

Goude, A., Ågren, O., 2014. Simulations of a vertical axis turbine in a channel. Renew. Energy 63, 477–485.

Hameed, M.S., Afaq, S.K., 2013. Design and analysis of a straight bladed vertical axis wind turbine blade using analytical and numerical techniques. Ocean Eng. 57, 248–255.

Healy, J., 1978. The influence of blade thickness on the output of vertical axis wind turbines. Wind Eng. 2, 1–9.

Howell, R., Qin, N., Edwards, J., Durrani, N., 2010. Wind tunnel and numerical study of a small vertical axis wind turbine. Renew. Energy 35, 412–422.

Islam, M., Fartaj, A., Carriveau, R., 2008. Analysis of the design parameters related to a fixed-pitch straight-bladed vertical axis wind turbine. Wind Eng. 32, 491–507.

Kamau, J.N., Kinyua, R., Gathua, J.K., 2010. 6 years of wind data for marsabit, kenya average over 14 m/s at 100 m hub height; an analysis of the wind energy potential. Renew. Energy 35, 1298–1302.

Kooiman, S., Tullis, S., 2010. Response of a vertical axis wind turbine to time varying wind conditions found within the urban environment. Wind Eng. 34, 389–401.

Lanzafame, R., Mauro, S., Messina, M., 2013. Wind turbine {CFD} modeling using a correlation-based transitional model. Renew. Energy 52, 31–39.

Li, Y., Calisal, S.M., 2010. Three-dimensional effects and arm effects on modeling a vertical axis tidal current turbine. Renew. Energy 35, 2325–2334.

Makridis, A., Chick, J., 2013. Validation of a {CFD} model of wind turbine wakes with terrain effects. J. Wind Eng. Ind. Aerodyn. 123 (Part A), 12–29.

Mcintosh, S.C., 2009. Wind Energy for the Built Environment (Ph.D. thesis). University of Cambridge.

McIntosh, S., Babinsky, H., Bertenyi, T., 2008. Unsteady power output of vertical axis wind turbines operating within a fluctuating free-stream. In: Forty-sixth AIAA Aerospace Sciences Meeting and Exhibit, Reno, Nevada.

McTavish, S., Feszty, D., Nitzsche, F., 2013a. Evaluating reynolds number effects in small-scale wind turbine experiments. J. Wind Eng. Ind. Aerodyn. 120, 81–90.

McTavish, S., Feszty, D., Sankar, T., 2013b. Steady and rotating computational fluid dynamics simulations of a novel vertical axis wind turbine for small-scale power generation. Renew. Energy 41, 171–179.

Monteiro, J.P., Silvestre, M.R., Piggott, H., André, J.C., 2013. Wind tunnel testing of a horizontal axis wind turbine rotor and comparison with simulations from two blade element momentum codes. J. Wind Eng. Ind. Aerodyn. 123, 99–106.

Mullen, J., Hoagg, J.B., 2013. Wind turbine torque control for unsteady wind speeds using approximate-angular-acceleration feedback. In: Decision and Control (CDC). In: IEEE Fifty-second Annual Conference on Decision and Control, IEEE 2013 , pp. 397–402.

Nobile, R., Vahdati, M., Barlow, J.F., Mewburn-Crook, A., 2014. Unsteady flow simulation of a vertical axis augmented wind turbine: a two-dimensional study. J. Wind Eng. Ind. Aerodyn. 125, 168–179.

Pourrajabian, A., Mirzaei, M., Ebrahimi, R., Wood, D., 2014. Effect of air density on the performance of a small wind turbine blade: a case study in iran. J. Wind Eng. Ind. Aerodyn. 126, 1–10.

Qunfeng, L., Jin, C., Jiangtao, C., Ning, Q., Danao, L.A.M., 2011. Study of cfd simulation of a 3-d wind turbine. In: International Conference on Materials for Renewable Energy & Environment (ICMREE), 2011, vol. 1, IEEE, pp. 596–600.

Raciti Castelli, M., Englaro, A., Benini, E., 2011. The darrieus wind turbine: proposal for a new performance prediction model based on cfd. Energy 36, 4919–4934.

Refan, M., Hangan, H., 2012. Aerodynamic performance of a small horizontal axis wind turbine. J. Sol. Energy Eng. 134, 021013.

Roh, S.-C., Kang, S.-H., 2013. Effects of a blade profile, the Reynolds number, and the solidity on the performance of a straight bladed vertical axis wind turbine. J. Mech. Sci. Technol. 27, 3299–3307.

Rossetti, A., Pavesi, G., 2013. Comparison of different numerical approaches to the study of the h-darrieus turbines start-up. Renew. Energy 50, 7–19.

Sasson, B., Greenblatt, D., 2010. Effect of steady and unsteady slot blowing on a vertical axis wind turbine. In: Twenty-eighth AIAA Applied Aerodynamics Conference, Chicago, IL, AIAA Paper, volume 4406, pp. 2010.

Sayed, M.A., Kandil, H.A., Shaltot, A., 2012. Aerodynamic analysis of different wind-turbine-blade profiles using finite-volume method. Energy Convers. Manag. 64, 541–550.

Scheurich, F., 2011. Modelling the Aerodynamics of Vertical-axis Wind Turbines (Ph.D. thesis). University of Glasgow.

Scheurich, F., Brown, R.E., 2013. Modelling the aerodynamics of vertical-axis wind turbines in unsteady wind conditions. Wind Energy 16, 91–107.

Sheldahl, R.E., Klimas, P.C., 1981. Aerodynamic characteristics of seven symmetrical airfoil sections through 180-degree angle of attack for use in aerodynamic analysis of vertical axis wind turbines, Technical Report, Sandia National Labs., Albuquerque, NM (USA).

Song, Q., Lubitz, W.D., 2014. Design and testing of a new small wind turbine blade. J. Sol. Energy Eng. 136.

Staelens, Y., Saeed, F., Paraschivoiu, I., 2003. A straight-bladed variable-pitch vawt concept for improved power generation. In: ASME 2003 Wind Energy Symposium, American Society of Mechanical Engineers, pp. 146–154.

Tai, F.-Z., Kang, K.-W., Jang, M.-H., Woo, Y.-J., Lee, J.-H., 2013. Study on the analysis method for the vertical-axis wind turbines having darrieus blades. Renew. Energy 54, 26–31.

Untaroiu, A., Wood, H.G., Allaire, P.E., Ribando, R.J., 2011. Investigation of self-starting capability of vertical axis wind turbines using a computational fluid dynamics approach. J. Sol. Energy Eng. 133, 041010.

Vahdati, M., Nobile, R., Barlow, J., Mewburn-Crook, A., 2011. Dynamic stall for a vertical axis wind turbine in a two-dimensional study. World Renew. Energy Congr. 15.

Wakui, T., Yokoyama, R., 2013. Wind speed sensorless performance monitoring based on operating behavior for stand-alone vertical axis wind turbine. Renew. Energy 53, 49–59.

Yen, J., Ahmed, N.A., 2013. Enhancing vertical axis wind turbine by dynamic stall control using synthetic jets. J. Wind Eng. Ind. Aerodyn. 114, 12–17.